Atomically Resolved Carrier Recombination at Si(111)-(7 × 7) Surfaces

R. J. Hamers and K. Markert
IBM T.J. Watson Research Center, Yorktown Heights, New York 10598
(Received 7 August 1989)

The local potential created by photoexcited electron-hole pairs at the surface of clean and partially oxidized Si(111)-(7×7) surfaces is probed with a scanning tunneling microscope. Strong reductions in the surface photovoltage on the 15–20-Å length scale are observed due to localized surface recombination centers. The dependence of the local photovoltage on illumination intensity allows recombination effects to be distinguished from band bending. Virtually all defects on Si(111)-(7×7) increase the recombination rate by destroying the two-dimensional order and increasing the coupling between surface and bulk states.

PACS numbers: 73.25.+i, 61.16.Di, 72.40.+w, 73.30.+y

The recombination of electrons and holes at semiconductor surfaces has been a subject of great scientific and technological importance. A fundamental concept in theories of recombination, in both the bulk[1,2] and at surfaces,[3,4] has been the presumed existence of localized "trapping centers," which dominate the recombination kinetics. The kinetics of photoexcited carriers at surfaces can be probed via the surface photovoltage (SPV) effect.[5–7] Conventional SPV measurements probe a large surface area and have therefore been unable to directly study the influence of trapping centers and other surface inhomogeneities, which affect both the equilibrium surface electronic structure and the nonequilibrium carrier dynamics. In this study, we use scanning tunneling microscopy (STM) as a probe of the *local* surface-potential changes induced by optical excitation on clean and partially oxidized Si(111)-(7×7) surfaces. Measurements of the local SPV as a function of illumination intensity and of the position of the STM tip allow us to distinguish static band bending from dynamic recombination effects and provide new insight into the nature of recombination at clean and defected surfaces.

Samples were 0.1-Ω cm Si wafers, both *n* type (As doped) and *p* type (B doped), cleaned in ultrahigh vacuum as described previously.[8] In some experiments, these surfaces were exposed to 5×10^{-9} Torr oxygen for 10–45 s, to adsorb submonolayer coverages of oxygen. Samples were illuminated using a 10-mW He-Ne laser or a 100-mW multiline argon-ion laser. These produced similar results, except that the more powerful argon-ion laser was required to achieve saturation of the SPV effect. Results shown here were obtained with the argon laser. The *p*-polarized light impinged on the sample at 80° from the tip axis, with a beam diameter estimated at 150 μm. The complicated sample-tip geometry makes the fluence at the tip uncertain. As a result, quantitative comparisons can only be made between different locations within the same STM image, which necessarily experience the same fluence.

On silicon, a space-charge layer exists in the near-surface region which bends the valence and conduction bands such that at the surface, the band edges are nearly equidistant from the Fermi level.[9,10] The band bending is upward on *n*-type material and downward on *p*-type material, but variations in the magnitude arise from inhomogeneities in the surface electronic structure. Because of the electric field in the space-charge region, electron-hole pairs produced by optical illumination will separate, and the resulting *nonequilibrium* distribution of charge carriers produces a voltage at the surface which is probed with the STM tip.

One manifestation of this surface photovoltage effect is that plots of the tunneling current versus voltage on illuminated samples show a lateral shift compared to those measured in the dark. Figure 1 shows that on illuminated *p*-type samples a negative current is observed with zero applied bias. This is a result of downward band bending, which causes photoelectrons to accumulate at the surface. By applying a positive bias of 0.4 V, we can null the tunneling current and measure the potential at the location of tip. On *n*-type material similar results are obtained, except that the SPV is opposite in sign.

In order to probe the spatial variations in the SPV we implemented a tunneling potentiometry apparatus. The STM electronics are gated such that during the first part of the cycle a constant voltage V_{stab} is applied to the sample, and a feedback system (FB1) adjusts the tip

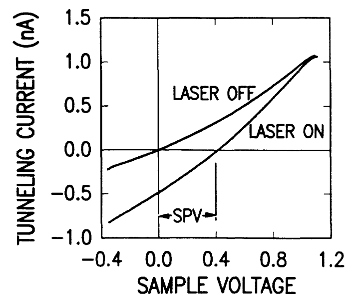

FIG. 1. Tunneling current vs voltage on *p*-type Si(111)-(7×7) with a stabilization voltage of +1.2 eV, demonstrating a lateral shift upon optical illumination.

© 1990 The American Physical Society

height to maintain a constant tunneling current. During the second part, FB1 is deactivated and a second feedback system (FB2) is activated; FB2 applies a voltage to the sample bulk to null the tunneling current. The output of FB1 is the conventional STM topography, while the output of FB2 is the local photovoltage (inverted in sign).

Figure 2 shows a representative topography and atomically resolved SPV measurements of a p-type Si(111)-(7×7) region ($V_{stab} = -1.0$ V) which includes a (7×7) domain boundary and several smaller defects. Figures 2(a) and 2(b) show the surface topography, as a gray-scale topview image [Fig. 2(a)] and as a three-dimensional representation [Fig. 2(b)]. In the top-view image 2(a) surface protrusions are white, and depressions black. In the three-dimensional representation [Fig. 2(b)], the perspective is keyed to the true height, while the local brightness is keyed to the local curvature (thereby presenting a realistic three-dimensional representation). Figures 2(c) and 2(d) are similarly keyed images showing the spatial variation in the surface photovoltage; white regions in Fig. 2(c) are regions of negative photovoltage (accumulation of electrons at the surface).

Comparing Fig. 2(a) with 2(c) shows that while some defects appear as protrusions and some as depressions in the topography, all defects strongly *decrease* the photovoltage signal compared to the ideal (7×7) regions. Other measurements both on n-type and p-type samples show that this is a general effect; more than 95% of all defects *decrease* the SPV signal for a diameter of ≃20–25 Å around each defect. Large defects often cause the SPV to be reduced by a factor of 20 or more; additionally, within the (7×7) unit cell we observe small variations of ≃(5–10)% in the SPV signal, which will be discussed later. At the extreme right of each of frames [Figs. 2(a)–2(d)], the laser was blocked; we see that there is some thermal drift (primarily of the tip, observed as an apparent contraction of the surface height) in the topographic image [Figs. 2(a) and 2(b)] but atomic resolution is maintained. At the same time, we see that (1) the surface photovoltage drops to zero, (2) the residual SPV noise is less than 5-mV peak, and (3) the residual SPV noise is uncorrelated with the local topography as the tip continues to scan across the surface. This undeniably confirms that the results presented in Fig. 2 arise from a surface photovoltage effect.

We also rule out thermoelectric effects from two independent sources. First, on the basis of calculations[11] which predict a temperature rise of less than 3 K, producing a negligibly small potential change of less than 3 mV.[12] Secondly, from the thermal expansion upon illumination [observed in Figs. 2(a) and 2(b)], we can put a firm upper bound of ≃5 K (producing <5-mV thermoelectric potential) by assuming that all the expansion is from the sample.[13] Thus, these two independent methods demonstrate that thermoelectric effects are negligible here, and that the measured potentials arise *entirely* from the nonequilibrium carrier distributions produced by optical excitation.

Although the absolute photovoltage is a complicated function of the bulk optical and transport properties, most of these quantities are constant, so that the spatial variation in the SPV has two major contributions. The first is from variations in the local band bending due to inhomogeneities in the density of surface states; the second is from variations in the local recombination rate. The first of these is an electrostatic effect and should

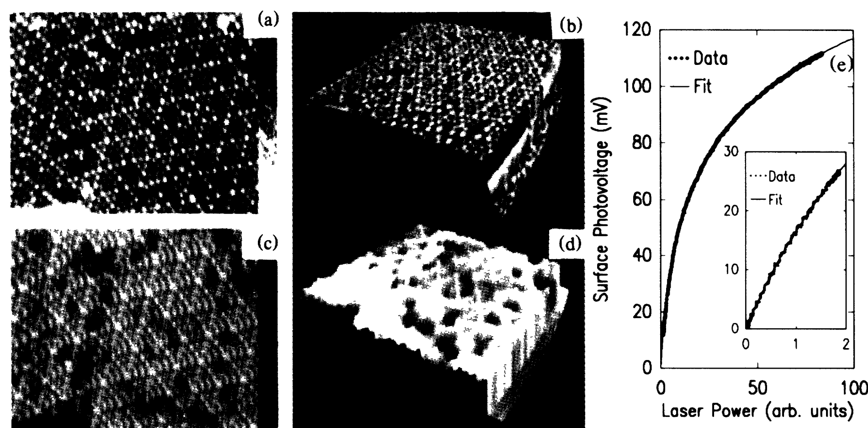

FIG. 2. Atomically resolved surface photovoltage measurements on p-type Si(111)-(7×7). The laser is blocked during the extreme right portion of each of frames (a)–(d). (a) Topographic image including a domain boundary and several small defects. (b) Three-dimensional representation of topography data. (c) Spatially resolved photovoltage image showing reduction in SPV around defects and at domain boundary. Laser power = 40 mW, average SPV signal = 110 mV while illuminated, gray scale range 50 mV. (d) Three-dimensional representation of photovoltage data. (e) Intensity dependence of SPV signal on clean Si(111)-(7×7) and a fit to the logarithmic function discussed in text.

have a characteristic length scale equal to the surface Debye length of $\simeq$50–85 Å, while the second is a purely kinetic effect. While a bulk Debye length of 50–85 Å is predicted, we expect the Debye screening length in the near-surface region to be significantly shorter than that in the bulk due to the surface segregation of the boron dopant, the increased density of carriers produced by the optical excitation, and the high density of surface states.

A quantitative distinction between band bending and recombination effects is obtained by measuring the SPV signal as a function of illumination intensity, I, providing information on the *kinetics* of the SPV effect. In Fig. 2(e), we show results obtained on a well-ordered Si(111)-(7×7) surface. The SPV varies almost linearly with I at low intensities (inset), but increases more slowly at higher intensities. At intensities where the density of photoexcited carriers δn is small compared to the total carrier density n, the SPV signal is predicted[3,4] to vary like $V_{\mathrm{SPV}} = A \ln(1+\delta n/n)$, where the constant A is determined by the local band bending. Since δn is proportional to the laser intensity I, this can be rewritten as $V = A^* \ln(1+BI)$. In Fig. 2(e), we show that our experimental data can be accurately fitted by a function of this form, indicating that this simple model accurately describes the essential physics of the situation. At much higher intensities, the density of photoexcited carriers can be larger than the density of dopant-induced carriers. Under those conditions the valence and conduction bands are driven flat[6,7,10] and the SPV signal is expected to "saturate" and become nearly independent of intensity.

At lower intensities where the simple model above is adequate, the second term in parentheses, BI, describes the ratio of the carrier generation rate to the recombination rate. Since the photoexcited carriers are generated throughout the absorption depth of $\simeq 10^4$ Å, their generation rate is independent of lateral position. As a result, spatial variations in the constant B can be attributed almost entirely to variations in the local surface recombination rate. Furthermore, values of "B" obtained at different surface locations (in a single STM scan) can be compared to provide quantitative measurements of the relative recombination rates.

In Fig. 3, we show the dependence of the SPV signals on the laser intensity I at specific surface locations. The topographic image [Fig. 3(a), $V_{\mathrm{stab}} = +1.0$ V] shows a (7×7) reconstruction with a defect induced by exposure to $\simeq$50 L (1 L$=10^{-6}$ Torr s) oxygen. Where the topography shows a well-ordered Si(111)-(7×7) reconstruction, the SPV image [Fig. 3(b)] shows a negative potential of 180 mV. At the defect, the photovoltage is reduced to less than half this value, while the tip retracts by $\simeq$1.5 Å. At the indicated locations, the tip scanning was stopped and the SPV was measured as a function of I. After each SPV vs I measurement the tip scanning was continued, so that measurements were obtained at several well-defined locations in each raster scan.

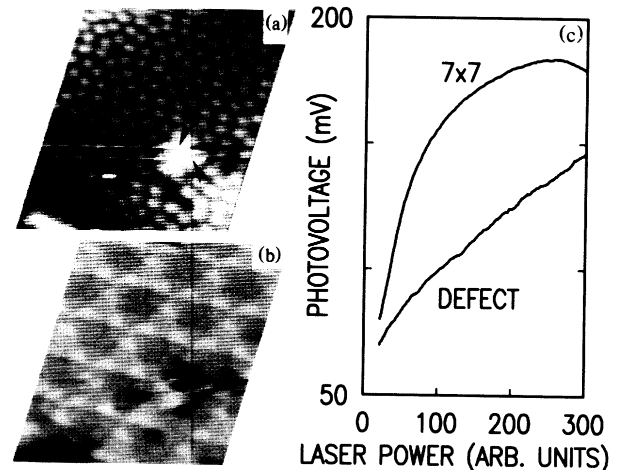

FIG. 3. (a) Topographic image of Si(111)-(7×7) with small defects. Arrows indicate the measurement points for (c). (b) Simultaneously acquired image of the local photovoltage. Average SPV = 170 mV, gray scale range 60 mV. (c) Dependence of photovoltage on laser intensity at the locations indicated in (a).

Figure 3(c) shows the dramatic difference between the shape of the curves obtained on the clean Si(111)-(7×7) surface and on the defect. On clean Si(111)-(7×7) the relation is logarithmic at low intensities [as in Fig. 2(e)], but at the higher intensities used here we also observe the anticipated saturation of the SPV effect as the bands are flattened and the SPV signal reaches a maximum of $\simeq$180 mV. At the defect, the dependence of the SPV on the laser intensity is much different, increasing much more slowly with laser intensity. Moreover, no saturation of the SPV signal is observed.

From an analysis of the shapes of the SPV vs I curves (as described above) we find that the recombination rate is $\simeq$4 times higher at this defect than on the ordered (7×7) surface. Similar measurements on other defects likewise demonstrate that they invariably increase the recombination rate and require much higher laser intensity to achieve the flat-band condition. From these results, we reach two main conclusions: (1) virtually all atomic-sized defects increase the recombination rate on the Si(111)-(7×7) surface; (2) almost all of the contrast in the SPV images arises from variations in the local recombination rate, rather than variations in the local (static) band bending.

Surface recombination is generally believed to be most efficient when the energy of the surface state lies in the middle of the bulk band gap.[3,4] Since the (7×7) surface has a very high density of surface states throughout the bulk band gap, it is quite surprising that defects almost universally increase the recombination rate even more. This is especially surprising for the samples exposed to oxygen, since oxidation reduces the density of midgap surface states[14] while we find that small oxidation-induced defects increase the recombination rate. We be-

lieve the explanation of these effects lies in the nature of the (7×7) surface states. These surface states (particularly the adatom states near the Fermi energy)[8] are essentially *two*-dimensional *Tamm* states with little overlap with the bulk valence or conduction bands. The disruption of this two-dimensional ordering results in increased coupling between the surface states and bulk states, making these defects more efficient recombination centers. This is to be contrasted to the recent results of Halas and Bokor,[15] where complete oxidation reduced the recombination rate compared to the clean Si(111)-(2×1) surface. There, complete oxidation reduced the recombination rate by eliminating all the midgap surface states. At our much lower exposures, oxidation increases the recombination rate on Si(111)-(7×7) by disrupting the two-dimensional ordering, thereby increasing the effective cross section for capturing electrons and holes.

We note that the value of ≃0.18 V obtained for the saturation SPV signal on the Si(111)-(7×7) surface is lower than the 0.63-V signal expected if the Fermi level is normally pinned midgap.[10] At these high intensities, there is a significant Dember potential, resulting from the higher mobility of electrons than holes. The Dember potential on *p*-type material is opposite in sign to the photovoltage, thereby reducing the observed potential at the high illumination intensities.

Somewhat more interesting is our observation of ≃10% variations in the observed photovoltage on the *atomic* distance scale. In Fig. 3, for example, the topographic image [Fig. 3(a)] shows no difference between faulted and unfaulted halves, and all twelve adatoms appear equivalent. Yet, the local photopotential [Fig. 3(b)] shows clear differences between faulted and unfaulted halves. The asymmetry in the photovoltage is quite similar to that found in earlier measurements of the spatially resolved density of states of Si(111)-(7×7) (Refs. 8 and 16) and indicates that the excess photoelectrons are preferentially located in the faulted half of the (7×7) unit cell. When the feedback loop is stabilized at negative sample bias (as in Fig. 2), the tunneling tip retracts slightly when in the faulted half of the unit cell (due to the higher density of states there), but the SPV signal is almost the same in both halves. Under these conditions, the increased photoelectron occupation of the faulted half is offset by the increased sample-tip separation (and hence, lower tunneling probability). This weak atomic-scale corrugation, and its dependence on the sample-tip separation (as determined by the stabilization voltage V_{stab}), has been confirmed numerous times on both *n*-type and *p*-type samples.

These measurements show that there is a weak distance dependence to the measured photopotential. Such a distance dependence cannot arise if the effect of illumination is simply to rigidly shift the surface potential with respect to the bulk. Rather, this distance dependence is a direct manifestation of the *nonequilibrium* distribution of electrons among the various bulk and surface states.[17] Conventional photovoltage measurements made with Kelvin probes or photoemission spectroscopy measure primarily the potential change at the surface, and are relatively insensitive to how the accumulation or depletion of charge carriers is distributed among the various energy states. Since the tunneling probability is a function of both the occupation and the energy of each state, however, tunneling measurements are also affected by the detailed distribution of the photoelectrons among the various energy states.

In summary, we have used STM to probe the nonequilibrium distribution of photoexcited charge carriers with atomic spatial resolution. Spatial maps of the SPV directly reveal the existence of localized recombination centers at (7×7) domain boundaries and oxidation-induced defects. Measurements of the SPV as a function of intensity allow us to unambiguously distinguish variations in the static band bending from variations in the local recombination rate. The combination of STM and optical excitation provides a unique method for identifying recombination centers and probing carrier transport at surfaces with atomic spatial resolution.

The authors would like to thank J. Clabes and J. Demuth for helpful comments. This work is supported in part by the U.S. Office of Naval Research.

[1]W. Shockley and W. T. Read, Phys. Rev. **87**, 835 (1952).

[2]R. N. Hall, Phys. Rev. **83**, 228 (1951).

[3]W. H. Brattain and J. Bardeen, Bell Syst. Tech. J. **32**, 1 (1953).

[4]D. T. Stevenson and R. J. Keyes, Physica (Utrecht) **20**, 1041 (1954).

[5]J. Lagowski, C. L. Balestra, and H. C. Gatos, Surf. Sci. **29**, 213 (1972).

[6]W. Mönch, P. Koke, and S. Krüger, J. Vac. Sci. Technol. **19**, 313 (1981).

[7]L. J. Brillson and D. W. Kruger, Surf. Sci. **102**, 518 (1981).

[8]R. J. Hamers, R. M. Tromp, and J. E. Demuth, Phys. Rev. Lett. **56**, 1972 (1986).

[9]F. G. Allen and G. W. Gobeli, Phys. Rev. **127**, 150 (1962).

[10]J. E. Demuth, W. J. Thompson, N. J. DiNardo, and R. Imbihl, Phys. Rev. Lett. **56**, 1408 (1986).

[11]M. Lax, J. Appl. Phys. **48**, 3919 (1977).

[12]S. M. Sze, *Physics of Semiconductor Devices* (Wiley, New York, 1981).

[13]In reality, we have strong evidence that most of the thermal expansion arises from the slender tip, not the sample.

[14]G. Hollinger and F. J. Himpsel, J. Vac. Sci. Technol. A **1**, 640 (1983).

[15]N. J. Halas and J. Bokor, Phys. Rev. Lett. **62**, 1679 (1989).

[16]R. J. Hamers, R. M. Tromp, and J. E. Demuth, Surf. Sci. **181**, 346 (1987).

[17]W. Kuhlmann and M. Henzler, Surf. Sci. **99**, 45 (1980).

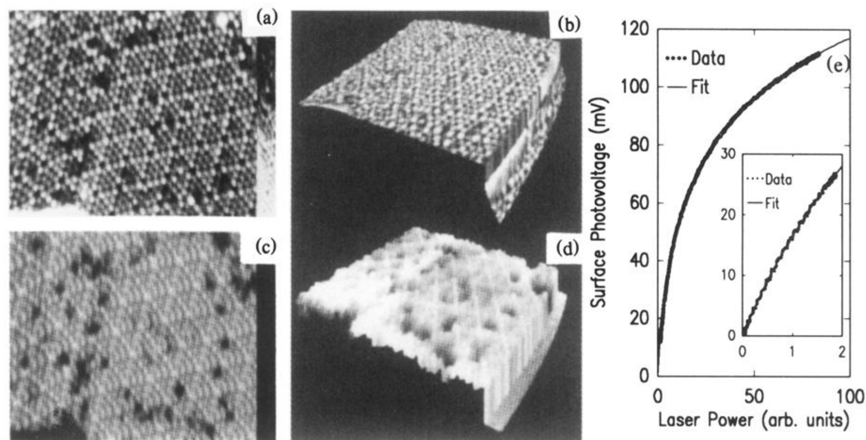

FIG. 2. Atomically resolved surface photovoltage measurements on *p*-type Si(111)-(7×7). The laser is blocked during the extreme right portion of each of frames (a)–(d). (a) Topographic image including a domain boundary and several small defects. (b) Three-dimensional representation of topography data. (c) Spatially resolved photovoltage image showing reduction in SPV around defects and at domain boundary. Laser power = 40 mW, average SPV signal = 110 mV while illuminated, gray scale range 50 mV. (d) Three-dimensional representation of photovoltage data. (e) Intensity dependence of SPV signal on clean Si(111)-(7×7) and a fit to the logarithmic function discussed in text.

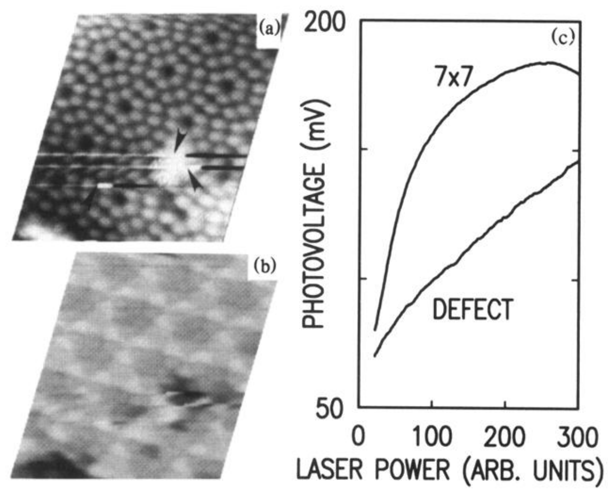

FIG. 3. (a) Topographic image of Si(111)-(7×7) with small defects. Arrows indicate the measurement points for (c). (b) Simultaneously acquired image of the local photovoltage. Average SPV = 170 mV, gray scale range 60 mV. (c) Dependence of photovoltage on laser intensity at the locations indicated in (a).